The Journal of Chemical Physics

RESEARCH ARTICLE | MAY 27 2022

A density functional theory based tight-binding study on the water effect on nanostructuring of choline chloride + ethylene glycol deep eutectic solvent

Sara Rozas ; Mert Atilhan ; Santiago Aparicio

J. Chem. Phys. 156, 204506 (2022)
https://doi.org/10.1063/5.0091665

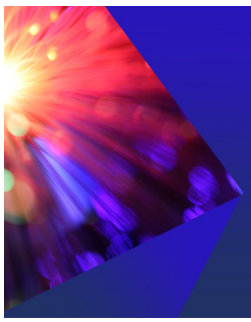

The Journal of Chemical Physics ARTICLE scitation.org/journal/jcp

A density functional theory based tight-binding study on the water effect on nanostructuring of choline chloride + ethylene glycol deep eutectic solvent

Cite as: J. Chem. Phys. 156, 204506 (2022); doi: 10.1063/5.0091665
Submitted: 16 March 2022 • Accepted: 3 May 2022 •
Published Online: 27 May 2022

Sara Rozas,[1] Mert Atilhan,[2,a)] and Santiago Aparicio[1,a)]

AFFILIATIONS

[1] Department of Chemistry, University of Burgos, 09001 Burgos, Spain
[2] Department of Chemical and Paper Engineering, Western Michigan University, Kalamazoo, Michigan 49008-5462, USA

[a)] **Authors to whom correspondence should be addressed:** mert.atilhan@wmich.edu and sapar@ubu.es

ABSTRACT

The effect of water on the properties of an archetypical type III deep eutectic solvent [choline chloride : ethyleneglycol (1:2)] is analyzed using *ab initio* molecular dynamics simulations in the 0 to 60 wt. % water content range. The properties of the mixed fluids are studied considering nanostructuring, intermolecular forces (hydrogen bonding), the energy of interactions, dynamic properties, and domain analysis. The reported results confirm that the change in the properties of the studied deep eutectic solvent is largely dependent on the amount of water. The competing effect of water molecules for the available hydrogen bonding sites determines the evolution of the properties upon water sorption. The main structural features of the considered deep eutectic were maintained even for large water contents; thus, its hydrophilicity could be used for tuning fluid physicochemical properties.

I. INTRODUCTION

The need for developing sustainable and efficient chemical products and processes has boosted interest in Deep Eutectic Solvents (DESs) both in industry and academia.[1] DESs are formed by mixing two or more compounds which at a specific mixing ratio leads to a significant decrease in the system melting temperature compared to those for pure components.[2] Therefore, depending on the components mixed to form the DES, five different types are considered (type I to type V).[3,4] Particular attention has been paid to type III DESs, formed by the combination of hydrogen bond acceptors (HBA, usually a salt) and hydrogen bond donors (HBD, which can be a variety of compounds, such as alcohols, organic acids, and sugars).[5,6] The interest in DESs, in particular to type III ones, is based on their suitable physicochemical properties, such as almost negligible vapor pressure, density, or polarity;[2,7] low cost;[8] biodegradability;[9] and low toxicity.[10] These suitable properties have led to the consideration of DESs for a plethora of applications[1,11] in areas such as drug delivery,[12,13] extraction,[14,15] gas separation,[16,17] synthesis,[18,19] or agri-food sector.[20]

DESs may be hydrophobic[21] or hydrophilic,[22] and in the case of the hydrophilic ones, the behavior of aqueous DES solutions has been considered.[23] Therefore, the behavior of DES aqueous solutions has been studied in the literature in terms of their structuring,[24,25] properties,[26] or applications.[27] Likewise, water in DESs can be treated as an impurity to eliminate or minimize,[23,28] or it could be added to tailor the physicochemical properties of the DESs.[29] Nevertheless, water has a significant effect on the structuring, intermolecular forces, and physicochemical properties of DESs.[30–33] Therefore, considering the hydrophilicity of many DESs, and thus their ability to absorb water from moisture from the ambient, it should be considered that a certain amount of water will be present in most DESs, thus affecting their properties.[25] The effect of water should be mainly based on its ability to act as both a hydrogen bond donor and an acceptor, thus being able to disrupt the HBA–HBD hydrogen bonding in type III DESs, which is one

of the roots of DES main properties.[34] The available literature has shown how the disruptive effect of water on DES properties is dependent on the water content, but despite the hydrogen bonding ability of water molecules, DESs can maintain most of their nanoscopic features up to high water contents[34] although effects are inferred even for low water contents for relevant macroscopic properties, such as viscosity.[35] The available studies on DESs plus water mixtures have shown three different composition regions:[31] (i) 0 to 30 wt. % of water, characterized by water dispersed in DES fluid; (ii) 30 to 50 wt. % of water, characterized by DES clusters dispersed in liquid water; and (iii) water content larger than 50 wt. % of water, which is formed by aqueous electrolyte solutions of DES components.

Nevertheless, for all the concentration ranges, water develops hydrogen bonding with the DES available sites.[36] Therefore, DES–water mixtures show complex structural features that are still not fully understood. For this purpose, molecular simulation techniques are a powerful tool to infer nanoscopic information and its link with mixed fluid behavior. A prototypical type III DES formed by the choline chloride, ChCl, and ethylene glycol, EG, ChCl:EG in 1:2 mol ratio (Fig. 1) is selected in this work for the analysis of its properties as a function of water content in a large concentration range. Ethaline has been considered for several technological applications,[37–41] and its nanostructuring and properties upon water mixing have been studied both experimentally[42,43] and theoretically.[25,44] Some theoretical results[44] showed minor changes in ethaline nanoscopic structuring up to a moderate water content, but the available experimental results showed non-negligible changes in the thermophysical properties.[43] Therefore, a deeper understanding of ethaline + water systems in a wide concentration range can provide valuable information on the effects of water sorption on DES properties. This work provides a theoretical study using *Ab Initio* Molecular Dynamics (AIMD) simulations using the density functional theory based-Tight Binding (DFT-TB) approach on ethaline + water mixtures in the 0 to 60 wt. % water content range. The study is based on a quantum chemistry approach. Thus, it does not suffer from the possible drawbacks of using classical molecular dynamics (CMD) simulations, which may depend on selecting a suitable force field. The reported results would allow analyzing the nanostructuring, intermolecular forces (hydrogen bonding), energy-related properties, and molecular arrangements, of the DES upon water sorption, and thus will give deeper insights into the effect of water in DES to assure the concentration ranges in which DES main features are maintained.

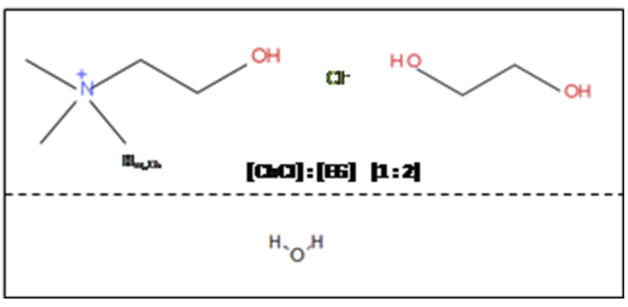

FIG. 1. Molecules composing the aqueous mixture considered in this work.

II. METHODS

Mixtures of [ChCl]:EG (1:2) plus water in the 0 to 60 wt. % water concentration range are studied using the simulation cages indicated in Table I. Cubic simulation boxes were initially built using Packmol program,[45] with the size of the boxes according to the experimental density data reported in a previous work.[25] These boxes were initially equilibrated using CMD simulations with MDynamix program using the force fields and methods previously reported[25] in the NPT ensemble at 303 K and 1 bar. The output structures of CMD simulations were used as initial input for AIMD simulations using the DFT-TB approach. AIMD/DFT-TB simulations were carried out using the DFTB + program.[46] The used Slater–Koster (SK) files correspond to the Third-Order Parameterization for Organic and Biological Systems (3OB).[47,48] The self-consistent calculations were carried out with 10^{-6} tolerance. The k-points meshes corresponded to a 4 × 4 × 4 distribution. AIMD simulations were carried out with a timestep of 1 fs for a total simulation time of 10 ps for each composition studied. The DTF-TB approach is ~100 to 1000 times faster than full DFT,[49] and the time required to carry out the simulations is dependent on the number of atoms considered. Table I indicates the number of total atoms in the considered simulations, which are in the 1050 to 2151 range. The analysis of the literature showed most of the DFT-TB for DES and related systems being carried out for systems containing less than 1000 total atoms with simulation times up to 100 ps.[49–51] Although 10 ps simulations were carried out in this work, it should be considered that, for the considered mixtures, the simulation boxes were previously equilibrated by CMD, which together with the low viscosity of the considered DES (39.78 mPa s[52]), which decreases upon water addition, assures that the considered simulation time is suitable for inferring the most relevant properties of the considered mixtures. AIMD simulations were developed in the NPT ensemble

TABLE I. Systems considered for NPT *Ab initio* molecular dynamics (AIMD simulations using DFT-TB) of ChCl:EG (1:2) + water mixtures wt. % stands for the weight percentage of water, x for water mole fraction, p for pressure, T for temperature, N for number of molecules, and n_{atoms} for the total number of atoms.

wt. % H_2O	x	N ([Ch][Cl])	N ([EG])	N ([H_2O])	n_{atoms}	p /bar	T/K
0	0	25	50	0	1050	1	303
1	0.13	25	50	4	1062	1	303
2	0.23	25	50	8	1074	1	303
3	0.31	25	50	11	1083	1	303
4	0.38	25	50	15	1095	1	303
5	0.44	25	50	19	1107	1	303
10	0.62	25	50	41	1173	1	303
15	0.72	25	50	65	1245	1	303
20	0.79	25	50	92	1326	1	303
25	0.83	25	50	122	1416	1	303
30	0.86	25	50	157	1521	1	303
35	0.89	25	50	197	591	1	303
40	0.91	25	50	244	1641	1	303
50	0.94	25	50	367	1782	1	303
60	0.96	25	50	550	2151	1	303

TABLE II. Domain analysis for molecular entities in ChCl:EG (1:2) + water mixtures. The domain count is reported with domain volume (D-Vol) and surface (D-Surf) as well as the isoperimetric quotient (Q^{peri}).

	$[Ch]^+$				Cl^-			
wt. % H_2O	Domain count	D-Vol/Å^3	D-Surf/Å^2	Q^{peri}	Domain count	D-Vol/Å^3	D-Surf/Å^2	Q^{peri}
1	1.0	140 451.1	28 511	0.31	20.8	1283	456	0.71
5	1.0	142 631	28 803	0.32	20.7	1141	462	0.68
10	1.0	140 345	28 255	0.30	27.8	700	341	0.67
15	1.1	127 677.2	27 537	0.21	396.1	87	87	0.70
20	1.6	93 725	28 988	0.24	410.3	25	81	0.72
25	2.8	50 244	25 996	0.38	384.5	53	84	0.73
30	4.9	23 889	20 521	0.54	399.2	47	78	0.74
35	8.5	14 027	14 141	0.60	400.8	36	60	0.75
40	23.5	4 162	3 914	0.64	422.4	38	67	0.76
50	70.5	1 301	1 280	0.59	441.9	34	62	0.77
60	7.2	8 598	3 096	0.55	22.4	350	215	0.69
	EG				Water			
wt. % H_2O	Domain count	D-Vol/Å^3	D-Surf/Å^2	Q^{peri}	Domain count	D-Vol/Å^3	D-Surf/Å^2	Q^{peri}
1	1.0	202 569	30 804	0.40	3.8	1 135	563	0.62
5	1.0	195 658	31 302	0.38	10.1	2 559	875	0.60
10	1.1	174 733	38 864	0.37	20.3	3 521	1 166	0.59
15	1.0	142 212	66 999	0.35	123.3	423	481	0.65
20	2.0	92 269	58 760	0.35	78.1	1 040	1 108	0.68
25	2.8	55 608	39 672	0.44	42.7	2 337	2 382	0.71
30	4.6	29 505	25 769	0.50	25.8	4 627	4 526	0.70
35	6.3	22 934	17 717	0.55	10.6	8 589	14 695	0.67
40	10.4	13 613	12 137	0.59	6.1	27 292	27 623	0.63
50	24.3	4 283	4 123	0.64	1.7	154 402	88 988	0.44
60	3.0	37 781	10 777	0.44	1.0	209 690	138 415.1	0.30

at 303 K and 1 bar with temperature and pressure-controlled using the Nosé–Hoover thermostat and Berendsen barostat, respectively. The visualization and analysis of the AIMD output trajectories were carried out using the VMD[53] and TRAVIS[54] programs.

III. RESULTS AND DISCUSSION

The analysis of ethaline + water mixtures using AIMD was first carried out using Radial Distribution Functions (RDFs) for relevant atomic sites. As the structure of the DES is characterized by hydrogen bonding between the hydroxyl site in Ch and chlorine anion as well as the chlorine–hydroxyl sites in EG and EG–EG hydrogen bonding, the changes in the corresponding RDFs were studied in the 0 to 60 wt. % water content range (Fig. 2). Regarding the Ch–Cl interactions [Fig. 2(a)], the first peak corresponding to the hydrogen bonding does not suffer relevant changes neither in its position nor in its shape up to 30 wt. % water concentration. At a higher water content, and especially at 60 wt. %, the peak shifts toward lower distances. This behavior indicates Ch–Cl pairing in the whole composition range, with a minor water content effect. The change in the high water content may indicate the presence of smaller clusters, i.e., shorter cation–anion distances and thus stronger interactions. In the case of Cl–EG interaction [Fig. 2(b)], up to the 30 wt. % water content, the peak indicating hydrogen bonding remains almost unchanged, and only additional features such as second RDF peaks appear at 60 wt. %, which show the decrease of cluster size, i.e., their dispersion in a media with water as solvents. As the considered DES has 1:2 mol ratio, EG molecules may develop hydrogen bonding between those molecules interacting with the same Cl and with neighbor EG molecules, which is the reason of the two main peaks appearing in the corresponding RDFs, Fig. 2(c), with these peaks almost unchanged up to the 60 wt. % water content, with only the first peak shifting at the high water content, which agrees with the decrease of ethaline cluster sizes. The reported RDFs were integrated for the relevant peaks, N, showing the content of each type of atom around the central one [Fig. 3], thus leading to quantitative information on the composition of the corresponding solvation shells. Despite the minor changes in RDFs reported in Figs. 2(a)–2(c) for ethaline components, the N values in Figs. 3(a)–3(c) indicate non-linear evolution with increasing water content. In the case of Cl around oxygen atoms in Ch [Fig. 3(a)], minor changes are inferred in the 0 to 15–20 wt. % range, then a decrease in the 20 to 40 wt. %, and then again constant. This result points to three composition regions in which although, as indicated by RDFs in Fig. 2(a), Ch

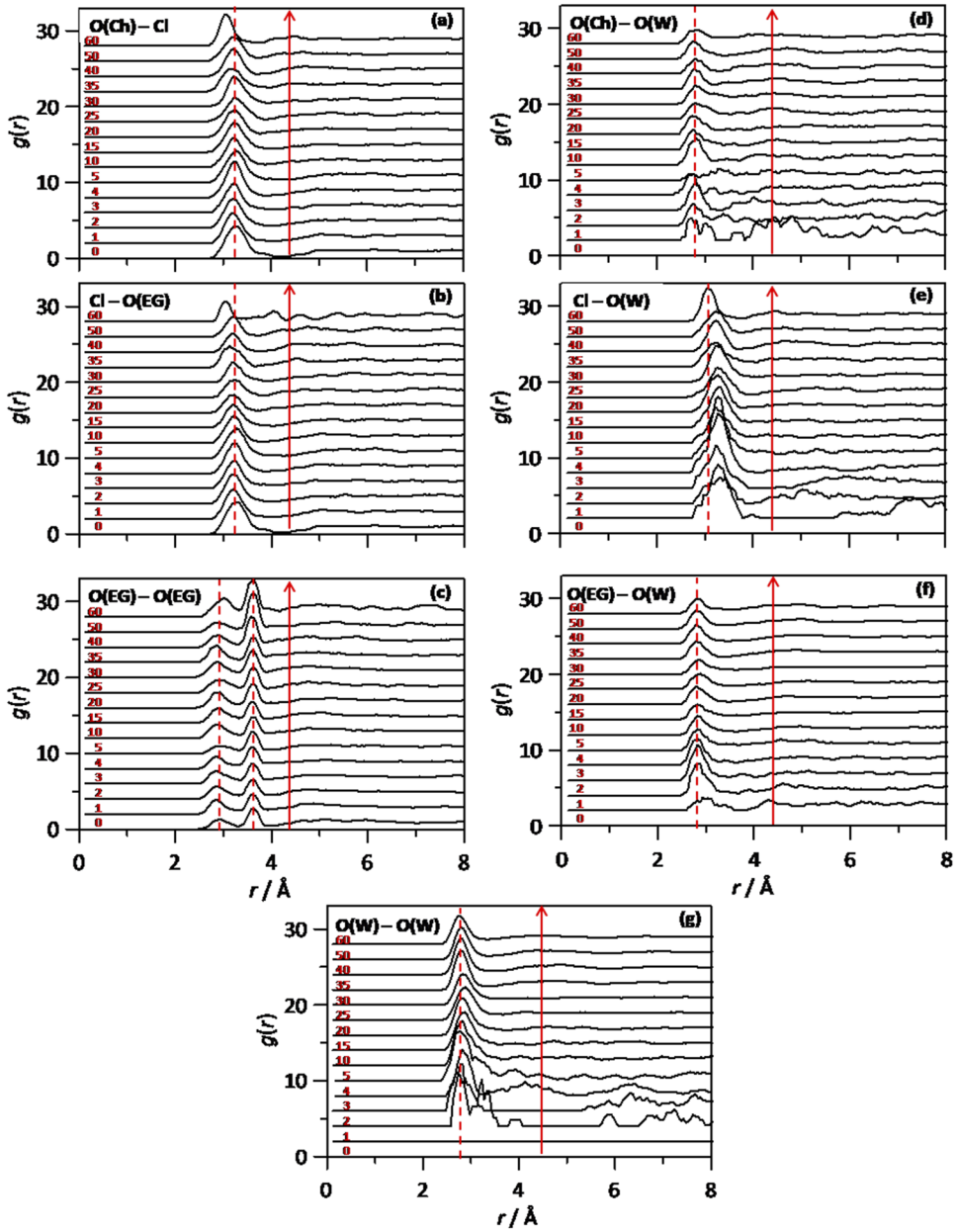

FIG. 2. Site–site radial distribution functions, $g(r)$, for the reported atomic pairs in ChCl:EG (1:2) + water mixtures at 303 K and 1 bar for different water content. Labels inside each panel indicate water content (wt. %). Arrows indicate increasing water content. Dashed lines show relevant peaks position. Panels: (a) Ch cation (O atom)–Cl anion, (b) Cl anion–EG (O atoms), (c) EG (O atoms) –EG (O atoms), (d) Ch cation (O atom) –water (O atoms), (e) Cl anion–water (O atoms), (f) EG (O atoms)–water (O atoms), and (g) water (O atoms)–water (O atoms).

and Cl ions remain hydrogen-bonded through the hydroxyl site, the number of anions around this site decreases because of the dilution effect.

For low water content mixtures, large DES clusters are surrounded by water molecules, with the size of DES clusters decreasing with increasing water content, thus leading to ionic pairs for water rich mixtures. In the case of Cl–EG, Fig. 3(b), the non-linear evolution of N, shows a decrease of EG molecules around the anion but with minor changes in the water content larger than 30 wt. %. For the case of EG–EG self-association [Fig. 3(c)], changes are remarkably lower than for Ch–Cl or Cl–EG, showing the large trend of EG molecules to remain self-associated even for the large water content. Regarding the association of water molecules with ethaline components, RDFs in Figs. 2(d)–2(f) indicate that water molecules interact with all the ethaline components even from the low water content, which is confirmed by the corresponding N values in Figs. 3(d)–3(f). Therefore, results in Figs. 3(a)–3(f) indicate that the solvation spheres around the hydrogen bonding sites in ethaline components upon water content increases are characterized by water molecules occupying these sites by the shifting of ethaline components (Ch, Cl, and EG). This is a non-linear effect accompanied by the self-aggregation of water molecules [Figs. 2(g) and 3(g)]. The non-linear

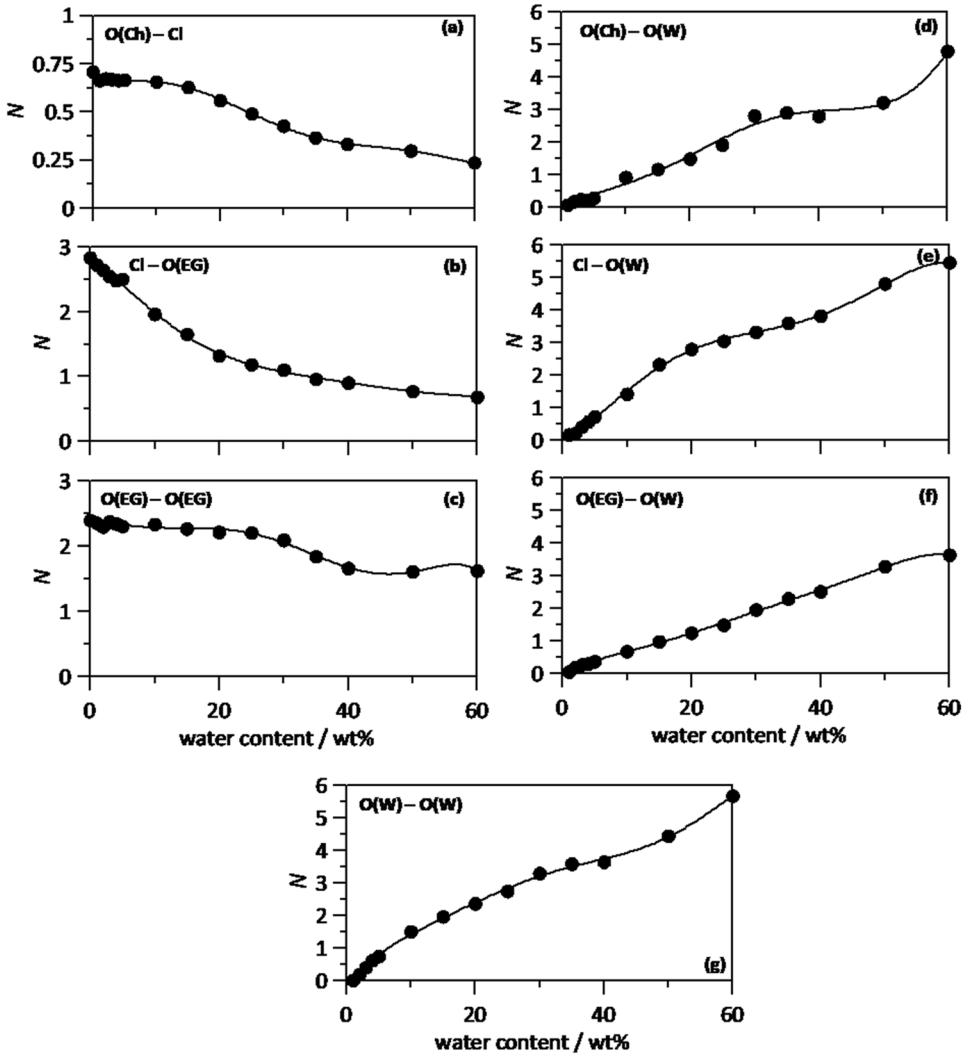

FIG. 3. Solvation numbers, *N*, obtained from the integration of radial distribution functions reported in Fig. 2, corresponding to the first solvation sphere (r = 4 Å), defined as the first minimum in the corresponding radial distribution function in ChCl:EG (1:2) + water from MD simulations at 303 K. Water content is indicated as wt. %. Panels: (a) Ch cation (O atom)–Cl anion, (b) Cl anion–EG (O atoms), (c) EG (O atoms)–EG (O atoms), (d) Ch cation (O atom)–water (O atoms), (e) Cl anion–water (O atoms), (f) EG (O atoms)–water (O atoms), and (g) water (O atoms)–water (O atoms).

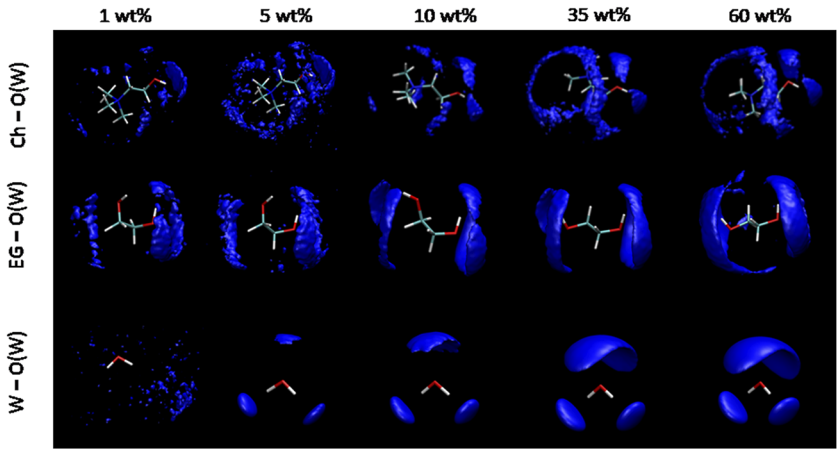

FIG. 4. Spatial distribution functions around central molecules in ChCl:EG (1:2) + water from MD simulations at 303 K. Water content is indicated as wt. %.

evolution with the water content of N for water self-aggregation [Fig. 3(g)] in which the three regions are well defined is remarkable: (i) increasing up to 20 wt. %, (ii) almost constant up to 30 wt. %, and (iii) a large increase for the water content larger than 30 wt. %. These three composition regions indicate (i) water molecules around the available hydrogen bonding sites in ethaline component with the increasing number of molecules around it and thus allowing both water–ethaline and water–water interactions (i.e., water in ethaline), (ii) the region between 20 and 30 wt. % characterized by the disruption of ethaline clusters and thus having minor effect on water self-association, and (iii) the dispersion of ethaline clusters in water leading to water as a solvent with increase of water–water interactions.

The distribution of water molecules around the main available hydrogen bonding sites is shown as the corresponding Spatial Distribution Functions (SDFs; Fig. 4). The increase in localized SDF caps around the hydroxyl groups in Ch and EG with the increase in the water content indicates how water molecules shift ethaline components from these sites. Likewise, the water increasing self-association is confirmed from the corresponding SDF even for the low water content, thus confirming the mechanism of ethaline solvation and disruption through the hydrogen bonding sites.

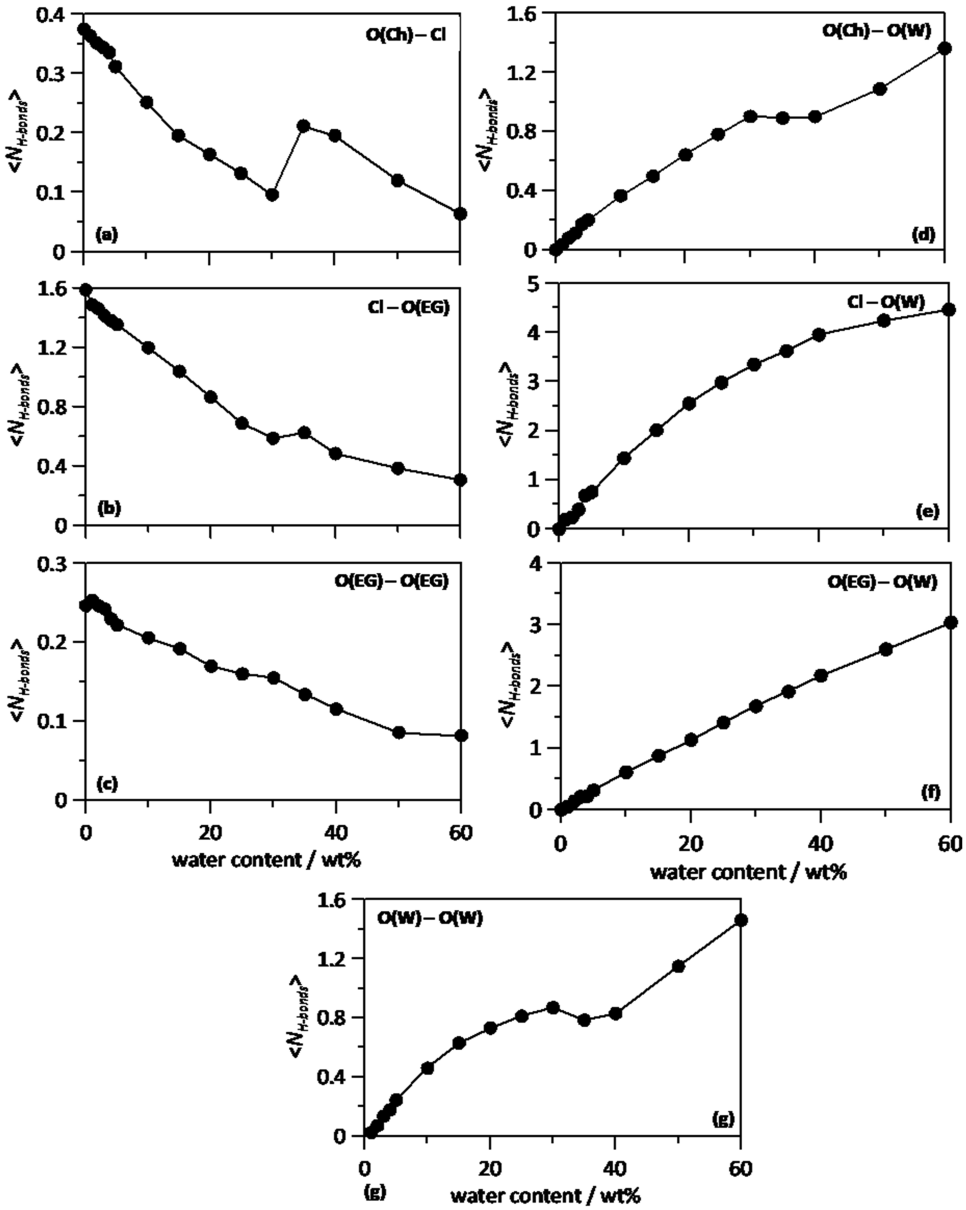

FIG. 5. Number of hydrogen bonds per molecule, $\langle N_{H\text{-}bonds} \rangle$, for the reported interacting pairs in ChCl:EG (1:2) + water from MD simulations at 303 K. Water content is indicated as wt. %. Panels: (a) Ch cation (O atom)–Cl anion, (b) Cl anion–EG (O atoms), (c) EG (O atoms)–EG (O atoms), (d) Ch cation (O atom)–water (O atoms), (e) Cl anion–water (O atoms), (f) EG (O atoms)–water (O atoms), and (g) water (O atoms)–water (O atoms).

Although RDFs, *N*, and SDFs have shown the mechanism of water–ethaline interactions, as the main features determining ethaline properties are based on the nature and extension of hydrogen bonding, it was quantified using a geometrical criterion as considering 60° and 3.5 Å for donor–acceptor orientation and separation for all the possible hydrogen bonding pairs (Fig. 5). The reported results indicate a decrease of hydrogen bonding between ethaline components accompanied by an increase in water–ethaline and water–water interactions. The evolution of all the properties with increasing water content is clearly non-linear. In the case of hydrogen bonding between ethaline components [Figs. 5(a)–5(c)], results show, for all the interacting pairs, a significant decrease up to roughly 20 wt. % water content and then minor changes in, any case, the perturbative effect of water on ethaline. Therefore, although RDFs in Fig. 2 indicate minor changes upon water increasing content, the *N* values in Fig. 3 and the number of hydrogen bonds per molecule in Fig. 5 suggest that water molecules disrupt the extension of ethaline self-hydrogen bonding, i.e., smaller ethaline clusters by competing effect on the ethaline hydrogen bonding sites. This is confirmed by the large trend of water molecules hydrogen bond with all ethaline components [Figs. 5(d)–5(f)]. Likewise, the water–water number of hydrogen bonds reported in Fig. 5(g) clearly indicates the three composition regions, with water molecules self-hydrogen bonding at the same time that interacting with ethaline hydrogen bonding sites (Fig. 4). Moreover, the extension of hydrogen bonding for most of the involved pairs indicates a sudden change of behavior for around 30 wt. % water content, mainly for those hydrogen bonds involving DES components. This sudden change may indicate a change from a DES-dominated fluid to a water-dominated fluid, in which DES molecules are dispersed into a surrounding water rich medium, leading to changes in DES self-aggregation. The characteristics of the developed hydrogen bonds involving water molecules

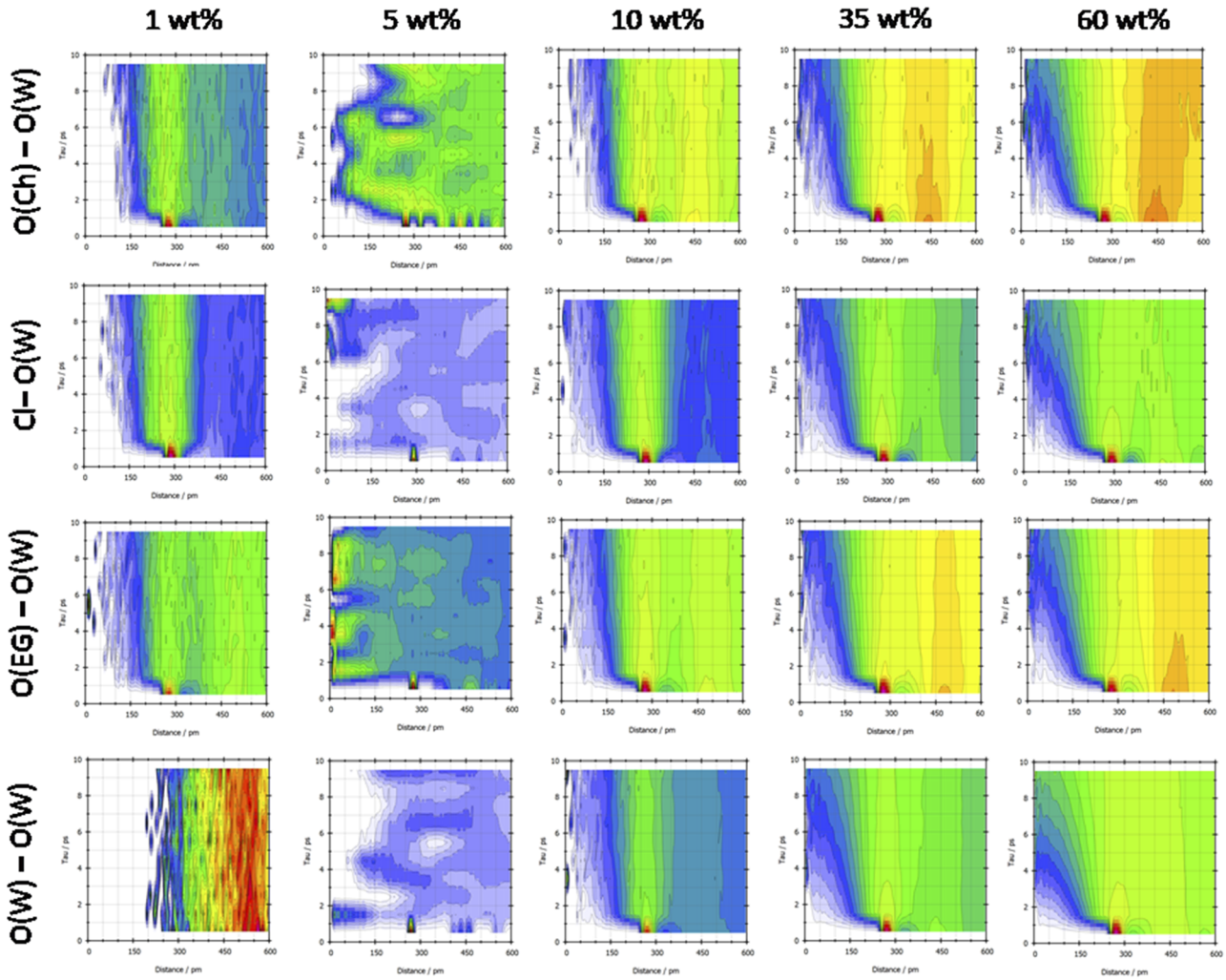

FIG. 6. Intermolecular Van Hove correlation function for the reported atomic pairs in ChCl:EG (1:2) + water from MD simulations at 303 K. The water content is indicated as wt. %.

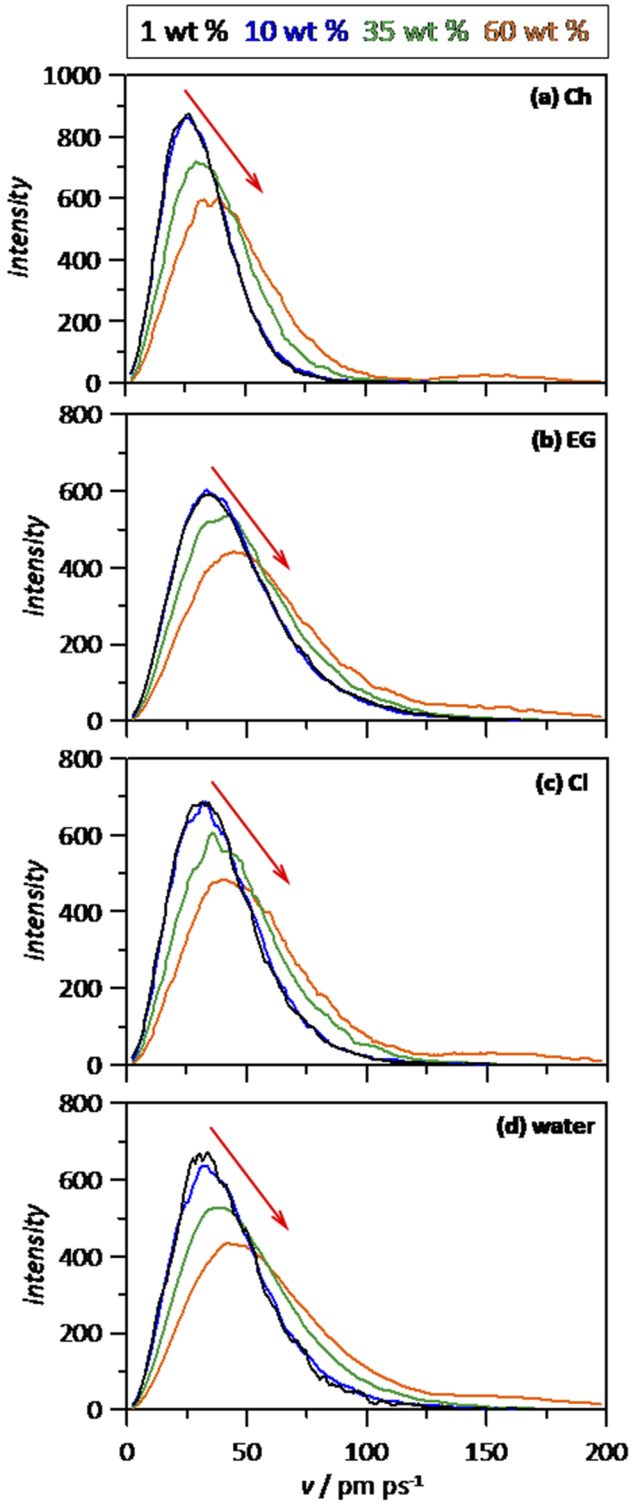

FIG. 7. Velocity, v, distribution functions for the reported molecules in ChCl:EG (1:2) + water from MD simulations at 303 K. Water content is indicated as wt. %. Panels: v for (a) Ch center-of-mass, (b) EG center-of-mass, (c) Cl center-of-mass, and (d) water center-of-mass.

are analyzed by the Van Hove correlation functions reported in Fig. 6. All the hydrogen bonds involving water molecules show the same dynamic features, with fast dynamics as indicated by the peaks (red spots) vanishing in few ps. Although water molecules show large hydrogen bonding with all ethaline sites, these interactions show quick reforming, and analogous behavior for water–water ones, in the whole studied water content range.

The changes in the developed hydrogen bonding in ethaline + water mixtures lead to changes in the dynamics of the involved molecules, which is quantified through the corresponding velocity distribution functions (Fig. 7). The reported results indicate changes in the velocity distribution peaks with increasing water content, although minor changes are inferred up to the 10 wt. % water content. For larger water contents, the maxima of the peaks shift toward faster velocities, and a widening of the peaks is produced, i.e., all the molecules move faster. It is remarkable that the velocity distribution curves for water molecules [Fig. 7(d)] show similar shapes as those for ethaline components, i.e., same maxima and width, which indicate coupling between water and ethaline molecules, as a result of the reported water–ethaline hydrogen bonding (Fig. 5). Likewise, the non-linear change of results in Fig. 7 for the maxima of the velocity distribution function with the water content also agrees with the sudden changes in hydrogen bonding extension for around 30 wt. % content of water (Fig. 5), which were justified as an evolution toward a water rich environment, thus allowing for faster molecular movements.

The interaction energy also quantifies the water–ethaline interaction (Fig. 8). The reported results show how water molecules efficiently interact with ethaline, agreeing with the developed hydrogen bonding (Fig. 5). Nevertheless, a non-linear evolution with the water content is inferred, with three well-defined composition regions, which agrees with the development of hydrogen bonding (Fig. 5). The region in Fig. 8 showing almost constant interaction energy indicates the transition region from ethaline dominated fluids, with larger ethaline cluster interacting with water, to water acting as a solvent with dispersed ethaline clusters, thus allowing for a larger number of water ethaline hydrogen bonds, Fig. 5, and therefore more significant interaction energy.

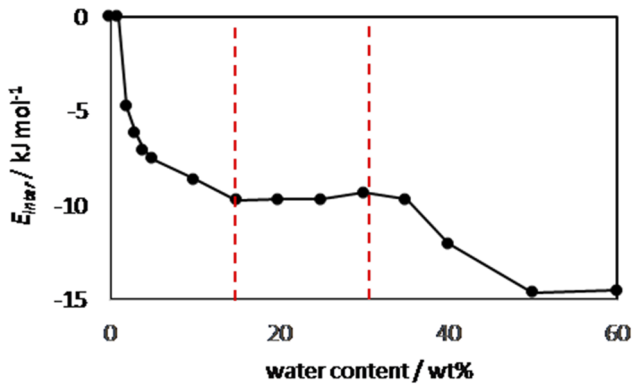

FIG. 8. Water–DES intermolecular interaction energy per water molecule, E_{inter}, in ChCl:EG (1:2) + water from MD simulations at 303 K. Water content is indicated as wt. %. Red dashed lines separate composition regions with different behavior.

The aggregation of molecules is analyzed using domain analysis[55] based on the Voronoi–method (Fig. 9). The domain-count number for the Cl anion shows a particular behavior [Fig. 9(a)]; for the water content up to 10 wt. %, a certain degree of anion self-aggregation is inferred, with the domain count around 25, but after that, the domain count increases showing isolated anions not interacting between them and only at the high water content, the domain count decreases. In the case of ethaline components [Fig. 9(b)], low domain counts are inferred (close to unity) up to the 20 wt.% water content, which indicates prevailing self-aggregation, and then, the domain count increases as a result of the water disruptive effect, indicating ethaline dispersion in the water solvent. A parallel behavior is inferred for EG molecules. The case of water [Fig. 9(b)] is of particular interest considering that the domain count evolves through maxima around 15 wt. % water content. For the low water content, a large water domain indicates water interacting with ethaline components (Fig. 5) but with minor interaction between them, i.e., small water clusters hydrogen-bonded with ethaline sites, but once the water concentration is large enough, water cluster sizes tend to increase, leading to an extended water network (domain count close to one) for the water content larger than 40 wt. %, i.e., water as solvent with dispersed ethaline clusters. The shape of the molecular clusters is quantified using the isoperimetric quotient, Q^{peri}, which indicates the sphericity of the molecular domains (the closer to unity the more spherical) [Fig. 9(c)]. The Q^{peri} values also evolve in a non-linear trend with increasing water content. Cl anions show the more spherical shape of their domains, whereas the Ch cation and EG show low sphericity of their domains with similar values and trends. Water domains are more spherical than those for Ch and EG, but its sphericity decreases as the water content increases, which agrees with the decrease of the water domain count, i.e., for the high water content, a continuous non-spherical domain is inferred

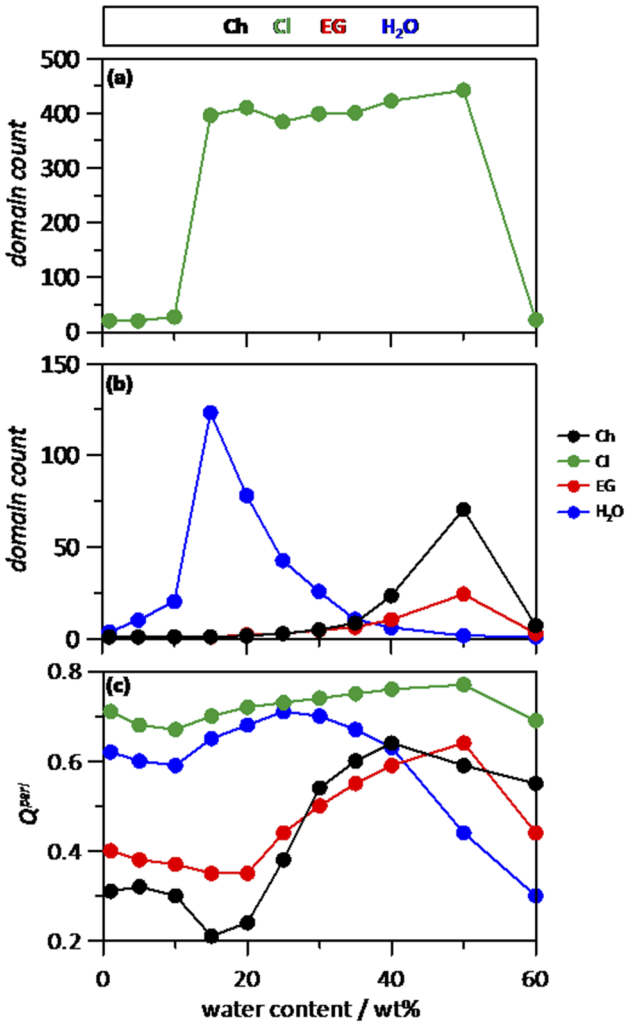

FIG. 9. Analysis of domain distribution in ChCl:EG (1:2) + water from MD simulations at 303 K. Panels: (a) domain count for Cl anion; (b) domain count for Ch cation, EG, and water molecules, and (c) isoperimetrical coefficient, Q^{peri}, for each type of molecule.

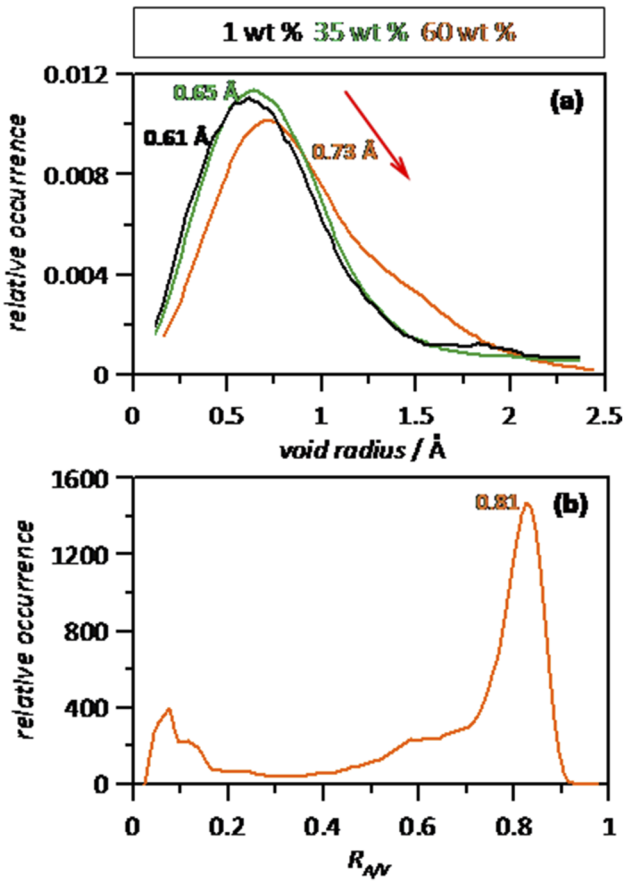

FIG. 10. Analysis of void distribution in ChCl:EG (1:2) + water from MD simulations at 303 K. Panels: (a) distribution of cavities as a function of cavity radius and (b) distribution of isoperimetrical ratio for cavities, $R_{A/V}$. Values inside each panel indicate the corresponding maxima; red arrow in panel (a) indicates increasing water content.

with a large number of ethaline dispersed domains. Moreover, the geometrical properties of the corresponding domains, area and volume, are reported in Table II for all the considered water contents. The geometrical parameters of domain components for all the ethaline components decrease with increasing water content (i.e., smaller clusters are inferred), accompanied by an increase of size for water domains, which agrees with the dispersion of ethaline in water for the large water content.

Additional analysis of ethaline + water systems is carried out considering the void distribution inferred from Voronoi analysis[56] (Fig. 10). The reported void distributions show a Gaussian shape for the considered water contents with maxima in the range 0.61 to 0.73 Å, shifting toward larger values with increasing water content [Fig. 10(a)], i.e., water addition increases the available free space in ethaline, but this effect is almost negligible up to the 35 wt. % water content. Regarding the distribution of void space (cavities), isoperimetrical ratio analysis for cavities was carried out, with values in the 0 to 1 range, values close to 0 indicating connected voids and those close to 1 showing isolated voids. The results in Fig. 10(b) indicate a maxima at 0.81, indicating poorly connected cavities. Therefore, the disrupting effect of water is only produced at the large water content, leading to slightly larger but poorly connected cavities, which would be produced by the dispersion of ethaline small clusters in the water solvent in contrast to lower water contents in which water molecules occupy sites around the available hydrogen bonding places in ethaline components, leading to very efficient molecular packing and thus minor expansion. Moreover, the domain count (Table II) for Ch and EG is 1 for water contents lower than 15 wt. %, which indicates an extended network for these species, as to indicate by the volume and surface of their corresponding domains, and thus, the main structural features of the considered DES are maintained up to high water contents.

IV. CONCLUSIONS

The properties of archetypical ethaline deep eutectic solvent with water mixtures and solutions are analyzed using *ab initio* molecular dynamics simulations. The reported results indicate that water has a big trend to be hydrogen-bonded with all the available sites in ethaline components (choline and chlorine ions and ethylene glycol), thus competing for these sites with ethaline components even for low water contents. This behavior decreases the hydrogen bonding between ethaline components but evolves in a non-linear way, with most of the ethaline features being maintained at concentrations as large as the 30 wt. % water content. Therefore, the structure of the solutions is characterized by ethaline clusters decreasing in size, with a lower degree of hydrogen bonding, as the water content increases, leading to small clusters dispersed in the water solvent. The perturbative effect of water also leads to an increase in the molecular mobility and to an increase of cavities, although this effect is only remarkable at high water contents. Therefore, water may be considered to modify properties of eutectics, such as ethaline, for purposes such as improving molecular mobility, i.e., lower viscosity, but maintaining the most relevant features of the fluid at a reasonable water content (lower than 20–30 wt. %). In contrast, for high water contents, the mixtures may be considered ethaline dispersed in the water solvent, i.e., losing the most relevant features of the deep eutectic solvent.

ACKNOWLEDGMENTS

This work was funded by the Ministerio de Ciencia, Innovación y Universidades (Spain, Project No. RTI2018-101987-B-I00). We also acknowledge SCAYLE (Supercomputación Castilla y León, Spain) for providing supercomputing facilities. The statements made herein are solely the responsibility of the authors.

AUTHOR DECLARATIONS

Conflict of Interest

The authors have no conflicts to disclose.

DATA AVAILABILITY

The data that support the findings of this study are available within the article.

REFERENCES

[1] B. B. Hansen, S. Spittle, B. Chen, D. Poe, Y. Zhang, J. M. Klein, A. Horton, L. Adhikari, T. Zelovich, B. W. Doherty, B. Gurkan, E. J. Maginn, A. Ragauskas, M. Dadmun, T. A. Zawodzinski, G. A. Baker, M. E. Tuckerman, R. F. Savinell, and J. R. Sangoro, "Deep eutectic solvents: A review of fundamentals and applications," Chem. Rev. **121**, 1232–1285 (2021).

[2] T. El Achkar, H. Greige-Gerges, and S. Fourmentin, "Basics and properties of deep eutectic solvents: A review," Environ. Chem. Lett. **19**, 3397–3408 (2021).

[3] L. Zamora, C. Benito, A. Gutiérrez, R. Alcalde, N. Alomari, A. A. Bodour, M. Atilhan, and S. Aparicio, "Nanostructuring and macroscopic behavior of type V Deep eutectic solvents based on monoterpenoids," Phys. Chem. Chem. Phys. **24**, 512–531 (2022).

[4] A. Mannu, M. Blangetti, S. Baldino, and C. Prandi, "Promising technological and industrial applications of deep eutectic systems," Materials **14**, 2494 (2021).

[5] A. Shishov, A. Pochivalov, L. Nugbienyo, V. Andruch, and A. Bulatov, "Deep eutectic solvents are not only effective extractants," TrAC Trend. Anal. Chem. **129**, 115956 (2020).

[6] F. M. Perna, P. Vitale, and V. Capriati, "Deep eutectic and their applications as green solvents," Curr. Opin. Green Sustainable Chem. **21**, 27–33 (2020).

[7] B. Gurkan, H. Squire, and E. Pentzer, "Metal-free deep eutectic solvents: Preparation, physical properties, and significance," J. Phys. Chem. Lett. **10**, 7956–7964 (2019).

[8] F. del monte, D. Carriazo, M. C. Serrano, M. C. Gutiérrez, and M. L. Ferrer, "Deep eutectic solvents in polymerizations: A greener alternative to conventional syntheses," ChemSusChem. **7**, 999–1009 (2014).

[9] L. I. N. Tomé, V. Baiao, W. da Silva, and C. M. A. Brett, "Deep eutectic solvents for the production and application of new materials," Appl. Mater. Today **10**, 30–50 (2018).

[10] X. Ge, C. Gu, X. Wang, and J. Tu, "Deep eutectic solvents (DESs)-derived advanced functional materials for energy and environmental applications: Challenges, opportunities, and future vision," J. Mater. Chem. A **5**, 8209–8229 (2017).

[11] F. Soltanmohammadi, A. Jouyban, and A. Shayanfar, "New aspects of deep eutectic solvents: Extraction, pharmaceutical applications, as catalyst and gas capture," Chem. Pap. **75**, 439–453 (2021).

[12] M. H. Zainal-Abidin, M. Hayyan, G. C. Ngoh, W. F. Wong, and C. Y. Looi, "Emerging frontiers of deep eutectic solvents in drug discovery and drug delivery systems," J. Controlled Release **316**, 168–195 (2019).

[13]S. N. Pedro, M. G. Freire, C. S. R. Freire, and A. J. D. Silvestre, "Deep eutectic solvents comprising active pharmaceutical ingredients in the development of drug delivery systems," Expert Opin. Drug Delivery **16**, 497–506 (2019).
[14]Y. Dai, G.-J. Witkamp, R. Verpoorte, and Y. H. Choi, "Natural deep eutectic solvents as a new extraction media for phenolic metabolites in *Carthamus tinctorius* L," Anal. Chem. **85**, 6272–6278 (2013).
[15]V. M. Paradiso, A. Clemente, C. Summo, A. Pasqualone, and F. Caponio, "Towards green analysis of virgin olive oil phenolic compounds: Extraction by a natural deep eutectic solvent and direct spectrophotometric detection," Food Chem. **212**, 43–47 (2016).
[16]M. Atilhan and S. Aparicio, "Review and perspectives for effective solutions to grand challenges of energy and fuels technologies via novel deep eutectic solvents," Energy Fuels **35**, 6402–6419 (2021).
[17]M. Atilhan and S. Aparicio, "Review on chemical enhanced oil recovery: Utilization of ionic liquids and deep eutectic solvents," J. Pet. Sci. Eng. **205**, 108746 (2021).
[18]H. Qin, X. Hu, J. Wang, H. Cheng, L. Chen, and Z. Qi, "Overview of acidic deep eutectic solvents on synthesis, properties and applications," Green Energy Environ. **5**, 8–21 (2020).
[19]J. D. Mota-Morales, R. J. Sánchez-Leija, A. Carranza, J. A. Pojman, F. del Monte, and G. Luna-Bárcenas, "Free-radical polymerizations of and in deep eutectic solvents: Green synthesis of functional materials," Prog. Polym. Sci. **78**, 139–153 (2018).
[20]A. Misan, J. Nadpal, A. Stupar, M. Pojic, A. Mandic, and R. Verpoorte, "The perspectives of natural deep eutectic solvents in agri-food sector," Crit. Rev. Food Sci. Nutr. **60**, 2564–2592 (2020).
[21]D. J. G. P. van Osch, C. H. J. T. Dietz, S. E. E. Warrag, and M. C. Kroon, "The curious case of hydrophobic deep eutectic solvents: A story on the discovery, design, and applications," ACS Sustainable Chem. Eng. **8**, 10591–10612 (2020).
[22]Y. Ma, Q. Wang, and T. Zhu, "Comparison of hydrophilic and hydrophobic deep eutectic solvents for pretreatment determination of sulfonamides from aqueous environments," Anal. Methods **11**, 5901–5909 (2019).
[23]C. Ma, A. Laaksonen, C. Liu, X. Lu, and X. Ji, "The particular effect of water on ionic liquids and deep eutectic solvents," Chem. Soc. Rev. **47**, 8685–8720 (2018).
[24]O. S. Hammond, D. T. Bowron, and K. J. Edler, "Innenrücktitelbild: The effect of water upon deep eutectic solvent nanostructure: An unusual transition from ionic mixture to aqueous solution," Angew. Chem. Ed. **129**, 9914–9917 (2017).
[25]S. Rozas, C. Benito, R. Alcalde, M. Atilhan, and S. Aparicio, "Insights on the water effect on deep eutectic solvents properties and structuring: The archetypical case of choline chloride + ethylene glycol," J. Mol. Liq. **344**, 117717 (2021).
[26]A. Jani, T. Sohier, and D. Morineau, "Phase behavior of aqueous solutions of ethaline deep eutectic solvent," J. Mol. Liq. **304**, 112701 (2020).
[27]C. Carlesi, N. Guajardo, R. Schrebler, and D. Vasquez-Sandoval, "Greener gas capture in deep eutectic solvents aqueous solutions: Performance in a dynamic condition," J. Cleaner Prod. **240**, 118240 (2019).
[28]D. Lapeña, L. Lomba, M. Artal, C. Lafuente, and B. Giner, "Thermophysical characterization of the deep eutectic solvent choline chloride:ethylene glycol and one of its mixtures with water," Fluid Phase Equilib. **492**, 1–9 (2019).
[29]Y. Dai, G.-J. Witkamp, R. Verpoorte, and Y. H. Choi, "Tailoring properties of natural deep eutectic solvents with water to facilitate their applications," Food Chem. **187**, 14–19 (2015).
[30]T. Zhekenov, N. Toksanbayev, Z. Kazakbayeva, D. Shah, and F. S. Mjalli, "Formation of type III deep eutectic solvents and effect of water on their intermolecular interactions," Fluid Phase Equilib. **441**, 43–48 (2017).
[31]L. Sapir and D. Harries, "Restructuring a deep eutectic solvent by water: The nanostructure of hydrated choline chloride/urea," J. Chem. Theory Comput. **16**, 3335–3342 (2020).
[32]A. Y. M. Al-Murshedi, H. F. Alesary, and R. Al-Hadrawi, "Thermophysical properties in deep eutectic solvents with/without water," J. Phys.: Conf. Ser. **1294**, 052041 (2019).
[33]Y. Wang, C. Ma, C. Liu, X. Lu, X. Feng, and X. Ji, "Thermodynamic study of choline chloride-based deep eutectic solvents with water and methanol," J. Chem. Eng. Data **65**, 2446–2457 (2020).
[34]Z. Naseem, R. A. Shehzad, A. Ihsan, J. Iqbal, M. Zahid, A. Pervaiz, and G. Sarwari, "Theoretical investigation of supramolecular hydrogen-bonded choline chloride-based deep eutectic solvents using density functional theory," Chem. Phys. Lett. **769**, 138427 (2021).
[35]G. Gydli, Z. Xu, and J. Pleiss, "Meta-analysis of viscosity of aqueous deep eutectic solvents and their components," Sci. Rep. **10**, 21395 (2020).
[36]P. Kumari, S. Shobhna, S. Kaur, and H. K. Kashyap, "Influence of hydration on the structure of reline deep eutectic solvent: A molecular dynamics study," ACS Omega **3**, 15246–15255 (2018).
[37]R. Bernasconi, G. Panzeri, G. Firtin, B. Kahyaoglu, L. Nobili, and L. Magagnin, "Electrodeposition of ZnNi alloys from choline chloride/ethylene glycol deep eutectic solvent and pure ethylene glycol for corrosion protection," J. Phys. Chem. B **124**, 10739–10751 (2020).
[38]E. Barrado, S. García, J. A. Rodríguez, and Y. Castrillejo, "Electrodeposition of indium on W and Cu electrodes in the deep eutectic solvent choline chloride-ethylene glycol (1:2)," J. Electroanal. Chem. **823**, 106–120 (2018).
[39]W. Li, J. Hao, S. Mu, and W. Liu, "Electrochemical behavior and electrodeposition of Ni-Co alloy from choline chloride-ethylene glycol deep eutectic solvent," Appl. Surf. Sci. **507**, 144889 (2020).
[40]M. Rogosic and Z. Kucan, "Deep eutectic solvents based on choline chloride and ethylene glycol as media for extractive denitrification/desulfurization /dearomatization of motor fuels," J. Ind. Eng. Chem. **72**, 87–99 (2019).
[41]M. E. Alañón, M. Ivanovic, A. M. Góme-Caravaca, D. Arráe-Román, and A. Segura-Carretero, "Choline chloride derivative-based deep eutectic liquids as novel green alternative solvents for extraction of phenolic compounds from olive leaf," Arabian J. Chem. **13**, 1685–1701 (2020).
[42]M. Busato, V. Di Lisio, A. Del Giudice, P. Tomai, V. Migliorati, L. Galantini, A. Gentili, A. Martinelli, and P. D'Angelo, J. Mol. Liq. **331**, 115747 (2021).
[43]A. Yadav, J. R. Kar, M. Verma, S. Naqvi, and S. Pandey, "Densities of aqueous mixtures of (choline chloride + ethylene glycol) and (choline chloride + malonic acid) deep eutectic solvents in temperature range 283.15–363.15 K," Thermochim. Acta **600**, 95–101 (2015).
[44]V. Alizadeh, F. Malberg, A. A. H. Pádua, and B. Kirchner, "Are there magic compositions in deep eutectic solvents? Effect of composition and water content in choline chloride/ethylene glycol from ab initio molecular dynamics," J. Phys. Chem. B **124**, 7433–7443 (2020).
[45]L. Martínez, R. Andrade, E. G. Birgin, and J. M. Martínez, "PACKMOL: A package for building initial configurations for molecular dynamics simulations," J. Comput. Chem. **30**, 2157–2164 (2009).
[46]B. Hourahine *et al.*, "DFTB+, a software package for efficient approximate density functional theory based atomistic simulations," J. Chem. Phys. **152**, 124101 (2020).
[47]M. Gaus, A. Goez, and M. Elstner, "Parametrization and benchmark of DFTB3 for organic molecules," J. Chem. Theory Comput. **9**, 338–354 (2013).
[48]M. Kubillus, T. Kubař, M. Gaus, J. Řezáč, and M. Elstner, "Parameterization of the DFTB3 method for Br, Ca, Cl, F, I, K, and Na in organic and biological systems," J. Chem. Theory Comput. **11**, 332–342 (2015).
[49]M. A. Addicoat, R. Stefanovic, G. B. Webber, R. Atkin, and A. J. Page, "Assessment of the density functional tight binding method for protic ionic liquids," J. Chem. Theory Comput. **10**, 4633–4643 (2014).
[50]T. Zentel and O. Kühn, "Properties of hydrogen bonds in the protic ionic liquid ethylammonium nitrate," Theor. Chem. Acc. **136**, 87 (2017).
[51]S. Spittle, D. Poe, B. Doherty, C. Kolodziej, L. Heroux, M. A. Haque, H. Squire, T. Cosby, Y. Zhang, C. Fraenza, S. Bhattacharyya, M. Tyagi, J. Peng, R. A. Elgammal, T. Zawodzinski, M. Tuckerman, S. Greenbaum, B. Gurkan, C. Burda, M. Dadmun, E. J. Maginn, and J. Sangoro, "Evolution of microscopic heterogeneity and dynamics in choline chloride-based deep eutectic solvents," Nat. Commun. **13**, 219 (2022).

[52]N. F. Gajardo-Parra, V. P. Cotroneo-Figueroa, P. Aravena, V. Vesovic, and R. I. Canales, "Viscosity of choline chloride-based deep eutectic solvents: Experiments and modeling," J. Chem. Eng. Data **65**, 5581–5592 (2020).
[53]W. Humphrey, A. Dalke, and K. Schulten, "VMD: Visual molecular dynamics," J. Mol. Graphics **14**, 33–38 (1996).
[54]M. Brehm, M. Thomas, S. Gehrke, and B. Kirchner, "TRAVIS—A free analyzer for trajectories from molecular simulation," J. Chem. Phys. **152**, 164105 (2020).
[55]M. Brehm, H. Weber, M. Thomas, O. Hollóczki, and B. Kirchner, "Domain analysis in nanostructured liquids: A post-molecular dynamics study at the example of ionic liquids," ChemPhysChem **16**, 3271–3277 (2015).
[56]S. Gehrke, R. Macchieraldo, and B. Kirchner, "Understanding the fluidity of condensed phase systems in terms of voids—Novel algorithm, implementation and application," Phys. Chem. Chem. Phys. **21**, 4988–4997 (2019).